

Full Length Research Paper

A physicochemical interpretation of the Turin Shroud imaging

Vitantonio Amoruso and Francesco Lattarulo*

Dipartimento di Elettrotecnica ed Elettronica, Politecnico di Bari, Via Orabona, 4 – 70125 Bari, Italy.

Accepted 12 July, 2012

The image impressed on the inner side of the Turin Shroud (TS) could be interpreted as the signature of a natural event. The fundamental working hypothesis adopted in this paper is that an accelerated physicochemical aging occurred on the topmost fibers of the cellulosic texture. This extremely superficial degradation is assumed as being originated by electrostatic discharges (ESD, often also referred to as partial discharges in gases, or corona effect) triggered by an exogenous electric field of seismic nature. On the basis of a purely electromagnetic treatment involving the time averaged Poynting vector and a generalized version of Lambert's cosine law, an analogical relationship between irradiance and surface electrostatic field is acknowledged. Accordingly, some new insight into the substantially undistorted features of the impressed human figure are gained and careful arguments aimed at circumventing some difficulties in the interpretation of the image formation are discussed. This is because light or other forms of electromagnetic radiation are elsewhere still indicated as possible causes of impression in substitution of a more realistic, inherently non-radiating, electrostatic agent. Distinctive of the present description is that some electrostatic, optical, material aging and geophysical properties are all together implicated in an interdisciplinary and self-consistent theoretical framework.

Keywords: Turin Shroud, image formation, electromagnetic radiation, electrostatics, Laplace equation, partial discharge, irradiance, Lambert cosine law.

INTRODUCTION

The authenticity of the Turin Shroud (TS) is subject to an ongoing criticism with a long history. However, a considerable amount of sustainable physicochemical arguments can be provided for a productive debate. This is the case, for example, when an electrostatic mechanism is claimed as being responsible for the image formation (Lattarulo, 1998; Fanti, 2010). The value of this hypothesis can be appreciated when a number of available observables (Adler, 2002; Fanti et al., 2010a; Fanti, 2010b) are taken into account. The subject is treated next, and followed by some joined optical considerations. Here, the Laplacian nature of the surface irradiance field and its formal analogy with an electrostatic field is acknowledged on the basis of a rigorous electromagnetic treatment (Lattarulo and Amoruso 2011). In this context, Lambert's cosine

law is discussed for nonplanar objects. The explanatory examples collected in this work are preliminary to a careful discussion on the TS imaging. The study especially emphasizes the electrostatic discharges (ESD), triggered by an exogenous electrostatic field, as a plausible impressing agent. The final intent of that is twofold: warning against questionable interpretations alongside radiation-based imaging mechanisms, and getting information from currently adopted electrostatic imaging techniques for a variety of applications (Kwark et al., 1994). The paper then fashions in part a report on the TS image-forming process triggered by a seismically originated electrostatic event. Some inexplicable observations made elsewhere (Fanti et al. 2004; Filas, 1983; Balossino, 1997; Danin, 2010; Frale, 2009) on the TS image are further considered and reasonably interpreted in the light of the proposed mechanism. Further substantiation to the ESD aging as a cause of the TS impression is consequently provided, thereafter some

*Corresponding author. E-mail: lattarulo@poliba.it.

concluding remarks.

BRIEF PHYSICOCHEMICAL REMARKS

Micro-scale

An ESD-originated physicochemical aging can ultimately result in a chemical reaction, since the physical transfer of energy (that is, kinetic, thermal or luminous nature) from the impinging filamentary plasma to the target is often far too faint to alter composition and morphology of exposed solid surfaces. This seems to be especially the case for the TS, even due to the poorly sensitive properties of a cellulosic fabric as a target. Electrochemical marks essentially manifest under form of superficial oxidation, dehydration and corrosion of the material side facing potently reacting chemical by-products (mainly ozone and acid formed by oxides of nitrogen in humid ambient). Careful surveys and special papers on the subject (Roth, 1959; Goldman et al., 1985; Van Blunt, 1994; Goldman et al., 1995), often tailored to technologists of insulating materials, show substantial accord with available analyses of the TS figure (Adler, 2002; Fanti et al., 2010). This special aging happens to be differently sensitive to a variety of experimental conditions, among which the electric field characteristics, surface material, gas properties, exposure time and discharge's modes parameters are the major factors. For example, when the energy of each elemental discharge of the overall plasma is below the corrosion onset level, only superficial oxidation, often accompanied by dehydration, are the effects manifested (this seems to be the case for the TS image). This threshold is detectable at the pulsating-to-nonpulsating (glow-type) discharge transition instant when, for example, an electrostatic field is somehow applied and increased by a laboratory set up. After this moment onwards, the oxidation process gives rise also to progressive erosion owing, of course, to the increasingly severe aging conditions established. In particular, whitish oxycellulose dust is removed from the target when it is made of vegetal fibers. When a fast time-varying electric field is applied, this is, for example, the case when the field obeys a sinusoidal law with a frequency of the order of some kHz and over (Font, 2006) or it is abruptly chopped (Waters, 1982), additional proliferation of unstable and vivid spark-type pulses is usually detected. In this case, confined degradation effects, however extraneous to the TS aging, are expected to take place somewhere. Conversely, when slowly-varying or static electric fields are applied, cutoff (or memory) effects due to charge accumulation on the surface of dielectric barriers are responsible for the pulsating character of the discharge and consequent absence of aging. Nevertheless, when the rate of ambient radioactivity is enhanced, the pulses are prone to merge in time, thus forming a glow capable to cause permanent modifications. Overall, it is clear that all the minute fea-

tures distinctive of the TS aging can hardly be reproduced without careful management of a number of experimental parameters. In spite of this, a pleasant observation is that fairly good records can be given when the experiment is carried out in specific natural conditions, namely within radon-invaded areas that closely resemble the physical circumstances here postulated for the TS imaging mechanism (de Liso, 2010; more detailed considerations will be mentioned in the course of this paper). In such experiments, conducted during tectonic activity, a stable and narrow-filament glow corona mode can manifest on conducting surfaces in spite of an essentially steady and moderate background electric field thus generated. Some second-order aging departures detected so far seem not detrimental to a seismoelectric imaging on the TS. Rather, they give stimulating arguments to undertake further experimentation ultimately aimed at proving that the TS figure is the result of specifiable and reproducible circumstances.

Macro-scale

A physical effect of paramount importance is that deriving from a careful observation of the TS image, even at naked eye. The subject deserves to be extensively treated separately by using some fundamentals of electromagnetism. As a result, an analogy between some optical and electrostatic performances, lately discovered elsewhere (Lattarulo and Amoruso 2011), is taken into account for an unprecedented electrostatics-based reading of the TS image. Consider that exploiting such an analogical property results in a recommended practice in computer graphics/vision for resolving object's rendering/recovering problems.

ELECTROMAGNETIC TREATMENT OF IRRADIANCE

A uniform plane wave (Figure 1) impinges at optical frequencies on a diffusely reflecting rough plane was placed in an unbounded domain filled by an aerial medium. A detector measures, irrespective of its position in the space, a surface reflectance governed by a simple formula. Accordingly

$$E = \rho E_0 \cos \gamma \quad (1)$$

reproduces Lambert's cosine law for the irradiance (Fanti et al., 2010), with ρ , E_0 and γ , denoting surface diffuse albedo (here assumed constant and less than unity) and incident plane wave's irradiance and inclination angle (referred to the surface normal, n), respectively. It is worth considering that an equivalent interpretation of the above formula is that the surface holds impenetrable ($\rho = 1$) to the incident plane wave provided the irradiance E_0 is virtually reduced to the quantity $E_0 \rho$. This remark is inherently irrespective of the system geometry since the

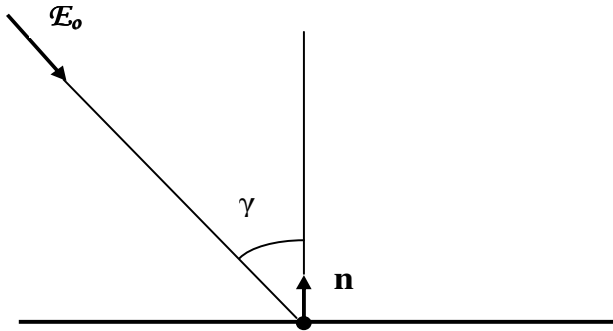


Figure 1. Plane illuminated with incidence angle γ and irradiance E_o .

relevant term, represented in Equation 1 by $\cos \gamma$ has been left uninvolved. As will be appreciated later on, the above equivalence is crucial in attempting a theoretical generalization of Equation 1 for the treatment of nonplanar objects. In fact, as it stands, the above formula should only be applied to the trivial case of an indefinitely extended plane. Therefore, there is still a need for Equation 1 to be revisited in view of typical computer graphics/vision applications involving nonplanar geometry. Irradiance perturbations ascribed to the average aspect of a generic body and to surface irregularities, when the body is isolated or in the presence of surrounding bodies, result quite neglected in Equation 1.

In consideration of the above objections, a purely electromagnetic approach has been adopted for giving a general method for irradiance assessment and discussing the limits of application for the traditional Lambert's cosine law. Use is made of the notion of time average (in the period) Poynting vector P_{ave} , the modulus of which corresponds, according to a radiometric terminology, to the locally reflected radiance E/π (Beckmann et al., 1878). Bear in mind that P_{ave} is the only part of the instantaneous power flow density, associated to a radiation field in a sinusoidal steady state, that holds physical meaning and is prone to practical employments (Stratton, 1941). The P_{ave} -field introduced is finite, continuous and vanishes at infinity, thus fully meets the prerequisite for being decomposed, according to Helmholtz's theorem, as follows

$$P_{ave} = -\nabla\phi + \nabla \times \Psi \tag{2}$$

Here, ϕ and Ψ are unspecified quantities respectively representing a curl-less scalar and a zero-divergence vector, while the negative sign assumed for the first addend means that this vector component is oriented towards ϕ drops. From Equation 2, $\nabla \cdot P_{ave} = -\nabla^2\phi$, so that rearranging this equality with;

$$\nabla \cdot P_{ave} + R_{ave} = 0 \tag{3}$$

easily gives the Poisson equation $\nabla^2\phi = R_{ave}$. In Equation

3, R_{ave} represents a time averaged dissipation addend that vanishes under specified circumstances. Provided these occur, $\nabla \cdot P_{ave} = \nabla^2\phi = 0$; that is, the P_{ave} -field is governed by a stationary Laplacian field. Therefore, setting $R_{ave} = 0$ causes $\text{grad } \phi = 0$ namely the potential ϕ to become harmonic subject to the boundary condition $\phi = \text{constant}$ all around, and inside, the body (Dirichlet condition). Bear in mind that virtually imposing lossless properties to the object has been made permissible by the previous ambivalent interpretation of the parameter ρ in Equation 1.

Introducing the identities $\text{div}(\phi \text{ grad } \phi) = \phi \text{ div grad } \phi + \text{grad } \phi \cdot \text{grad } \phi$ and $\text{grad } \phi \cdot n = \partial\phi/\partial n$ in the classical integral form of the divergence theorem

$$\int \text{div}(\phi \text{ grad } \phi) dV = \int \phi \text{ grad } \phi \cdot n dA \tag{4}$$

and remembering that $\text{div grad } \phi = 0$ gives

$$\int (\text{grad } \phi)^2 dV = \int \phi \partial\phi/\partial n dA \tag{5}$$

Equation 5 reduces to:

$$\int \phi \partial\phi/\partial n dA = \phi \int \partial\phi/\partial n dA = \int \partial\phi/\partial n dA = 0 \tag{6}$$

which proves how the net flux of $\partial\phi/\partial n$ through the closed surface of the body is zero. In conformity to the definition of irradiance that only applies to the illuminated side A_i of the body's entire surface A , a permissible reading of Equation 6 may be that the net flux of $\partial\phi/\partial n$ entering the body is zero owing to the perfect reflection of the irradiance wave impinging the surface of area A_i . It is worth noticing that the same equation applies to the case of a conducting object of same shape and dimension subject to purely electrostatic similar conditions. In this alternative case, the inwardly directed flux on the "illuminated" side of area A_i is indeed equal to, and formally assumes sign inverse of, the outwardly directed flux on the opposite "dark" side. Though, what matters in this investigation is the perfect analogy that has been established between irradiance and surface electric field on the exposed body side of area A_i .

The raised analogy allows a considerable amount of investigations, previously devoted to electrostatic applications, to be fruitfully exploited for some optical purposes. Some of those analogies led to rigorous verification that there is no unique dependence of the surface field on the local geometry, unless the body takes ellipsoidal or paraboloidal configuration (McAllister, 1990). In general, the problem becomes analytically intractable and a standard numerical Laplacian field solver unambiguously resolves the problem. A prominent property of Laplacian field problems subject to non-arbitrary boundary conditions is that they are well-posed as the required conditions of existence, uniqueness and continuity are indisputably met.

The special subject here treated rather compels to

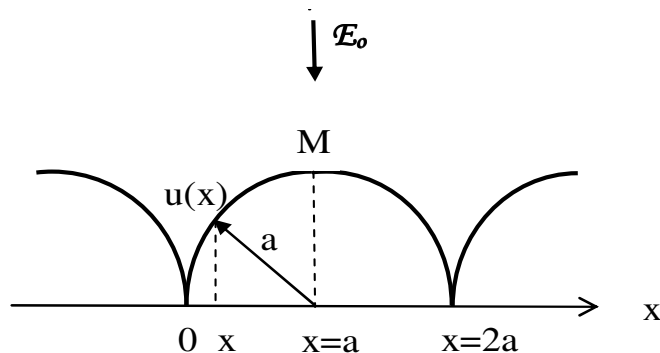


Figure 2. Corrugated sheet with semi cylindrical ridges of radius a . Position variable $u(x) = a \cos^{-1}(1-x/a)$ along the contour.

inspect the laid-on-plane E -pattern distributed on the illuminated surface of a nonplanar object, than its planar projection; the latter rather corresponding to the definition of image irradiance perceived by a receded observer. Of course, the laid-on-plane irradiance pattern generally appears as an enlarged and disfigured image of the object vision. However, the arguments next supplied will prove that the raised unpleasant perception is substantially circumvented when special conditions are met. As will be appreciated in the study, this is exactly the case for the TS figure observed on a plane, even assuming that the human body was tightly enveloped during the preliminary imaging process.

THEORETICAL EXAMPLES

A pair of analytically amenable case studies have been selected for introductory reasons. In the first example, an indefinitely extended parallel array of semi-cylindrical ridges is vertically illuminated according to Figure 2 (Lattarulo et al., 2011). The second example regards an unsophisticated ellipsoidal representation of a human body behaving as a scatterer or source (Figure 3). Only theoretical comments are made for such a simple model since they are only aimed at better acknowledging the quality of the subsequent complex application. In this final case, fully furnished with figures, an articulate mannequin composed by an assembly of 13 prolate and oblate ellipsoids, corresponding to as many large dimensioned anatomical blocks, is adopted. The required numerical calculation has been performed by a commercially available finite element package equipped with graphical facilities. The results are expressed in Figures 7 to 9 where a referential color scale is reported. In the pair of Figures 7, 8 and 9, the surface field is respectively referred to a uniform field of 1 V/m, in which the discharged body is embedded, and to a potential of 1 V assigned to the charged body. Color's code and gradation are everytime established by the program in an automatic fashion.

Ridges

According to Figure 2, the corrugation is exposed to a transversally propagating plane wave. The distribution law for the local irradiance $E(u)$ normalized to its maximum value $E(u=\pi a/2)$ (attained on the tip M of each ridge) obeys a simple formula that reads (Langton and Davy 1953).

$$E(u)/E(u=\pi a/2) = k F(u) \tag{7}$$

Where, u , F and k designate position variable on the curved contour, special geometry transformation function and proportionality constant, respectively. Consider that Equation 1 invariably simplifies $\cos \gamma$ provided the target reduces to a ridge in isolation on an infinite plate. This occurs since the complicated influencing mechanism that involves all the ridges simultaneously, disappears. For comparative reasons, the relevant curves are reported in Figure 3, where, owing to the bilateral symmetry of the pattern, the position variable u only runs on the semi-contour $O-M$ without loss of information. The pair of grey-gradated patterns depicted in Figure 4, represents planar image irradiances, as being perceived by an on-axis far enough apart detector. The patterns regard the cases of: a) a ridge in isolation and b) a ridge as member of corrugation. Corresponding patterns for the laid-on-plane surface irradiances, as were reconstructed by scanning in closed proximity to the semicircular contour, are reported in Figure 5. The remarkable differences between the relevant data prove that the laid-on-plane surface irradiance is, in the present example, a poor representation of an image irradiance in both the a) and b) cases.

Ellipsoid

Scatterer

With reference to Figure 6, the ellipsoid mimics a frontally illuminated human body. The uniform irradiance E_0 is thus directed along the x -axis, the semi-major axes $a \leq b \leq c$ being taken as a frame of reference (x,y,z) . For a 1.75-m tall, 80-kg weighting man, available empirical formulas (Mosteller, 1987) give a total surface area not exceeding 2 m^2 , here reduced to an outer value of 1.4 m^2 in conformity to the TS man's special posture. Therefore, anthropometric ratios $c/b = 3.2$ and $b/a = 2$ have been obtained for the equivalent model. According to previous remarks, the permissible application of the Lambert law to an ellipsoidal object,

$$E/E_M = \cos \gamma \tag{8}$$

$E = E(x,y,z)$ being the surface irradiance and $E_M = E(x=a, y=x=0) = E_0 \xi_x$. Of course, Equation 8 also represents the elliptic projection on the (y,z) -plane of the

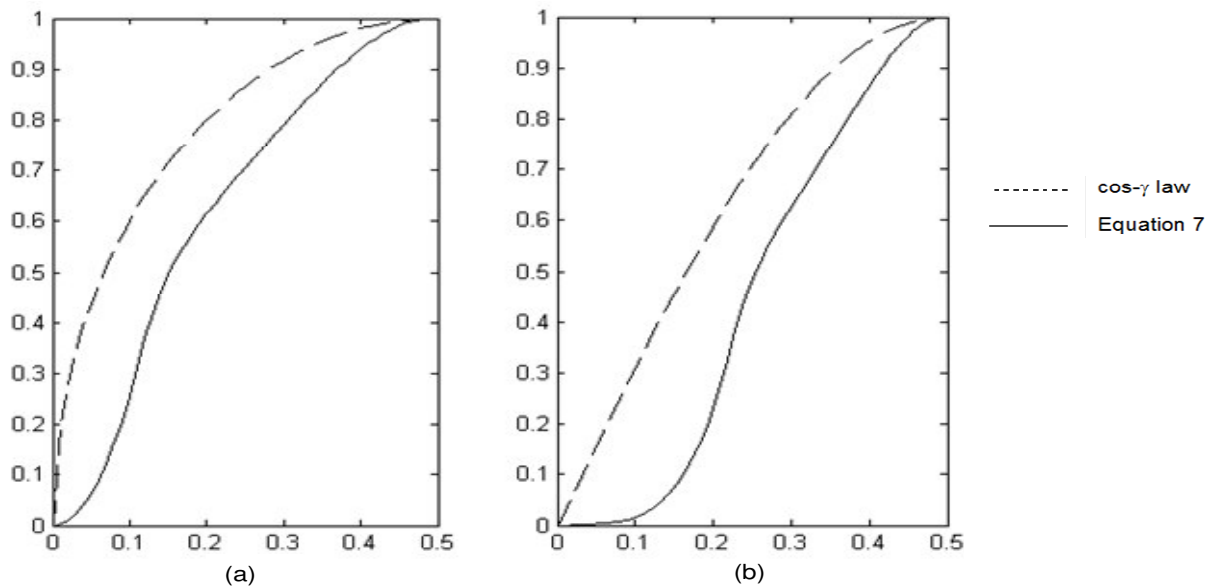


Figure 3. Normalized curves in function of x/a and $u(x)/u(x=\pi a/2)$. a) Surface irradiance projected on the plane; b) surface irradiance laid on the plane.

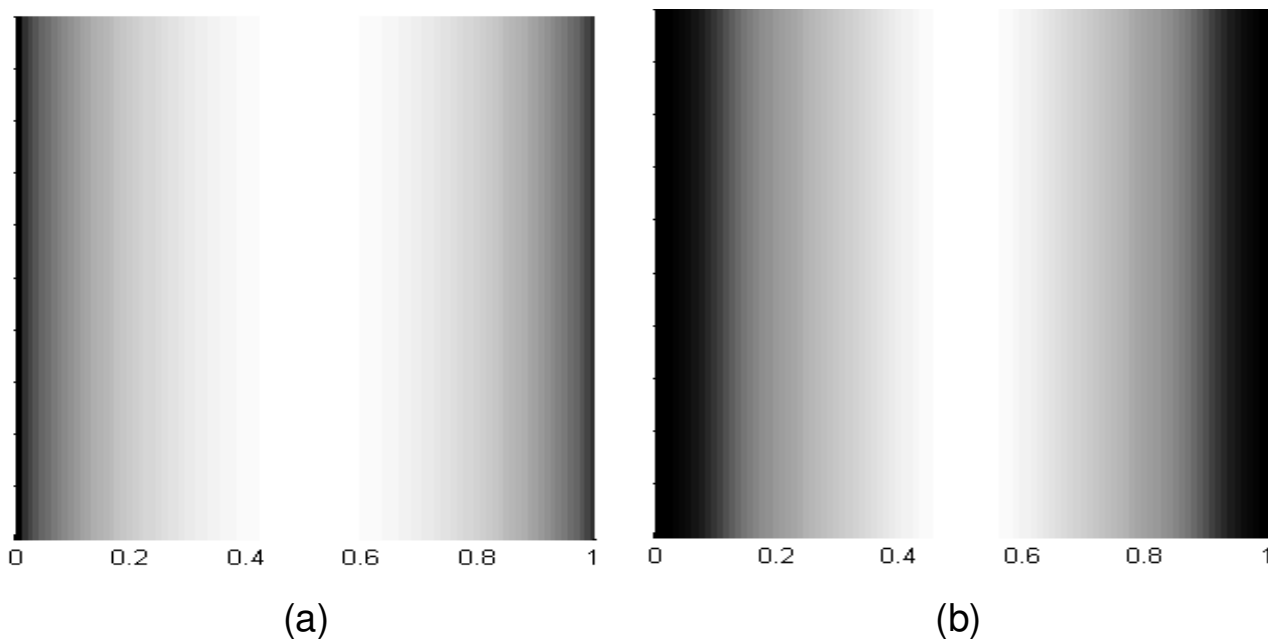


Figure 4. Grey-gradated image irradiance representation. a) Ridge in isolation; b) ridge as a member of corrugation. Numerical values: ratio $x/(2a)$ with $0 \leq x \leq 2a$ (shown in Figure 2).

surface irradiance. In other words, the above formula gives the elliptical image irradiance, of semi-major axes b, c , perceived by a distanced on-axis detector. For the sake of convenience, Equation 8 can be reformulated as follows:

$$E/E_M = [a (x^2/a^4 + y^2/b^4 + z^2/c^4)^{1/2}]^{-1} x/a \tag{9}$$

Using straightforward manipulations ultimately gives:

$$E/E_M \cong |x|/a \cong 1 \tag{10}$$

Provided $0 \leq |y|/b \leq 1/2$. The upper bound can physically represent the image/non-image boundary on a distanced recording affected by a given sensitivity threshold.

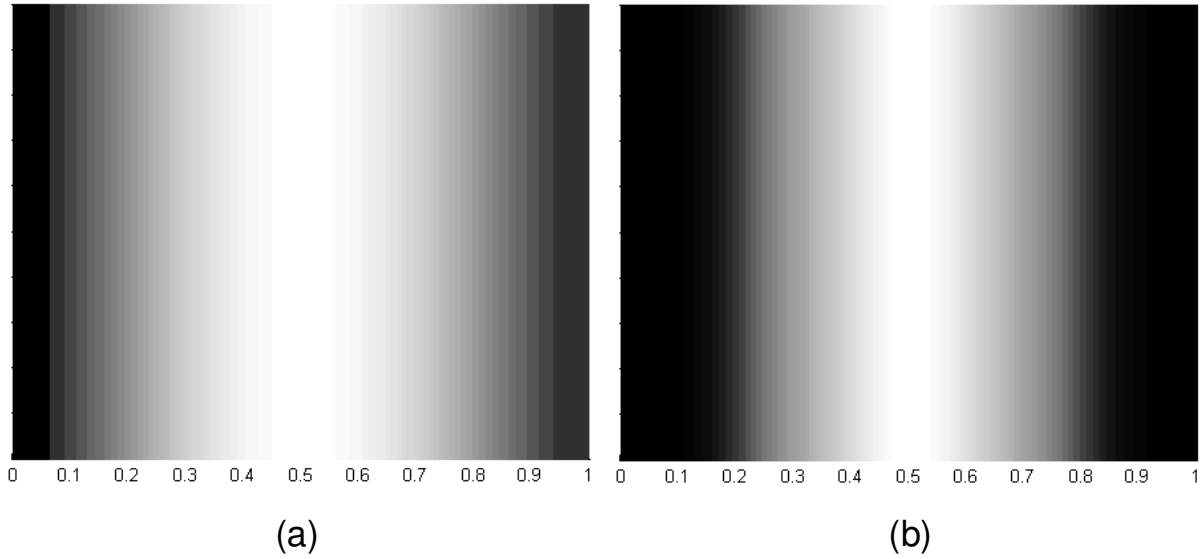


Figure 5. Grey-gradated laid-on-plane surface irradiance representation. a) Ridge in isolation; b) ridge as a member of corrugation. Numerical values: ratio $u(x)/u(x=2a)$ with $0 \leq x \leq 2a$ (shown in Figure 2).

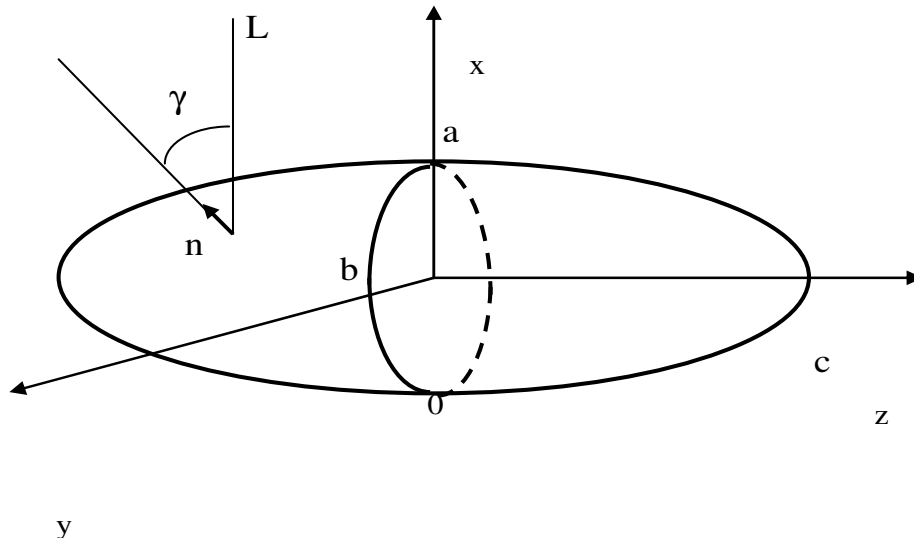


Figure 6. Ellipsoidal scatterer or source. Scatterer case: L both denotes line of incidence and sight for a uniform irradiance E_0 and distanced observer, respectively; surface irradiance dependent on $\cos \gamma$. Source case: L only denotes distanced observer's line of sight; no dependence of surface irradiance on $\cos \gamma$.

According to the analogy between irradiance and electric field, the same boundary can alternatively be ascribed to the sensitivity of the material film that fits the ellipsoidal conductor during the electrostatic impression. Equation 10 advises that the exposed side is so flat that E is allowed to slightly change within the above range. As an important consequence, the laid-on-plane elliptic figure appears nearly undistinguishable, as to image's quality and extension, from its projection on the (y,z)-plane (namely from the ellipsoid rendering).

Source

For a supplementary investigation, the above isolated body now assumes the role of radiating source. Again using the electrostatic analogy with a charged conducting ellipsoid (Stratton, 1941), gives

$$E/E_c = [a(x^2/a^4 + y^2/b^4 + z^2/c^4)^{1/2}]^{-1} \tag{11}$$

Where, E/E_c represents the surface irradiance normalized

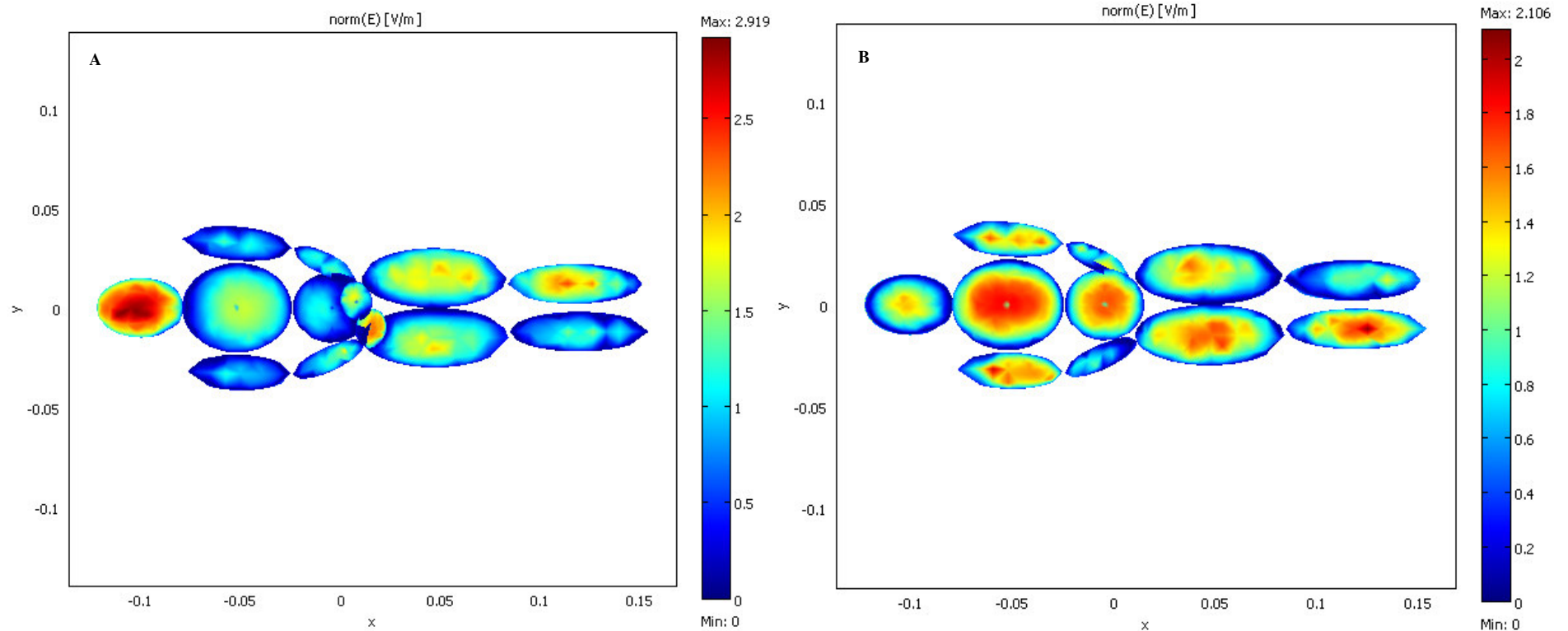


Figure 7. Electric field on a conducting multiple-ellipsoid model of man. Case study: Discharged floating body immersed in a frontally incident uniform field of 1 V/m.

to the value E_c on the central point of coordinates $x=a, y=z=0$. Accordingly, the laid-on-plane shadowing reverses now, thus resulting in a disfigured rendering of the ellipsoid features. This is mathematically explained because, contrary to Equation 9, Equation 11 is deprived of the multiplicative ratio x/a that plays the role of preventing the object to become progressively bright, instead of dark, towards the regions at larger curvature. On the other hand, the image irradiance projected on the (y,z) -plane is invariably governed by Equation 8 or 9, the irradiance being independent

of the line of sight for a diffusely emitting/reflecting surface.

Multiple-body model

The collection of images illustrated in Figure 7 refers to a conducting mannequin, in a supine attitude, that is isolated in the space and frontally exposed to a uniform electric field. The practical reasons explaining the importance of this simplified floating-body, for example, is extensively

examined subsequently in this study. The illustration sequenced in Figures 7 a to e shows the pattern of the electric-field modulus on the mannequin surface according to a distanced observer’s frontal, dorsal, lateral, podalic and cephalic visions. The same figures analogically describe planar image irradiances of the mannequin behaving as a diffusely reflecting target. The surface field changes in function of the geometry of, and mutual influence among, the single blocks. It is easy to verify in Figures 7a and b, how the more the elemental regions of the model are

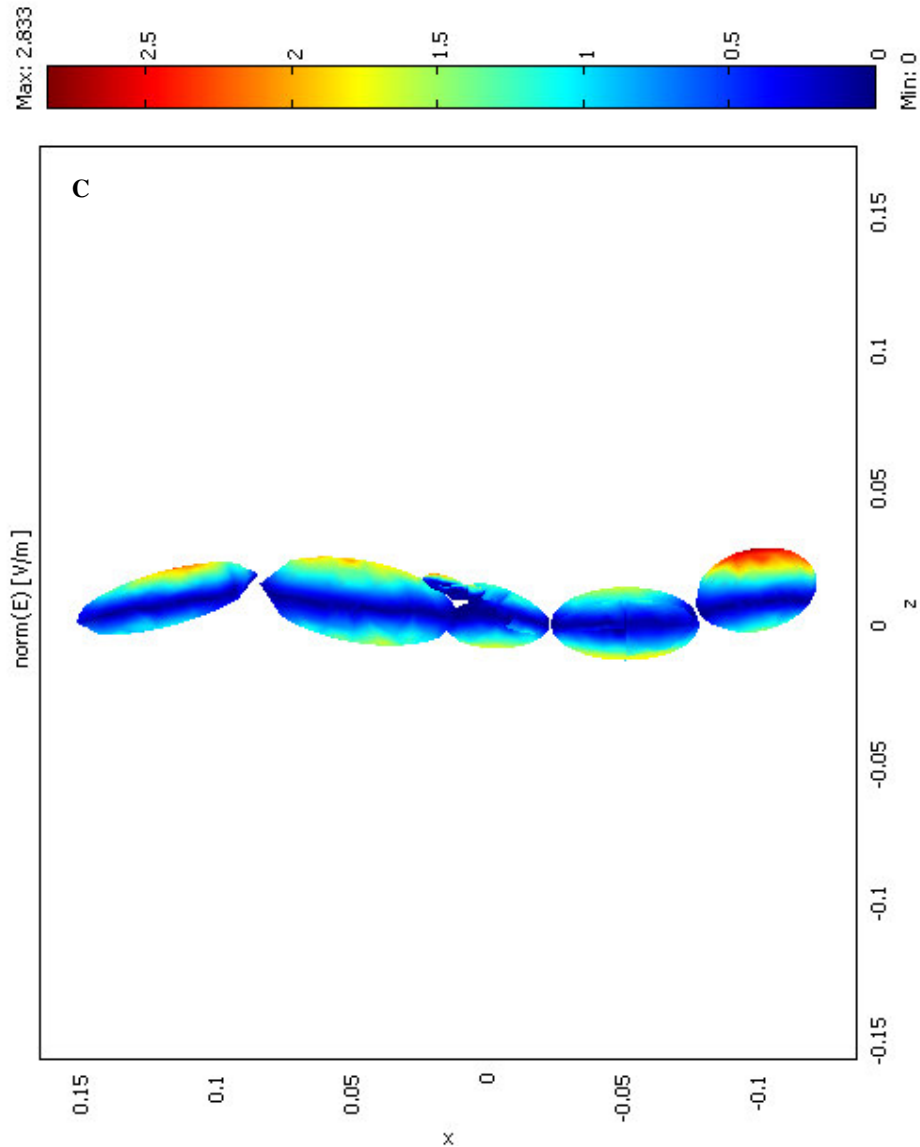


Figure 7. Contd.

prone to expand and protrude upwards and downwards, namely along the vertical direction of the exogenous field, the more they are stressed at the expenses of the depressed and lateral regions. Incidentally, it is worth observing how the field magnitude on the face exceeds the remaining parts all over the body. Of course, this description is substantiated by the given supplementary figures, even though the predominant reason for subset (c) to (e) to be added is to better display the existence of a vanishing-field strip longitudinally looping the body surface. Note, in this respect, the corresponding blue regions in Figures 7c, d, and e, respectively positioned on either side and at the poles of the body. Of course, the wide loop under examination causes the two separated and variously stressed figures, representative of the front

and rear of the body, to rather appear confined and distanced. Overall, the above performances are identical, in a qualitative sense, to those previously examined in "Scatterer" for the case of a single ellipsoid. When the human model is, for the sake of comparison, settled down on an indefinitely extended ground plane while the remaining geometrical and exposure conditions are left unaltered, then the surface field pattern changes dramatically. The difference can be appreciated in Figure 8, where a more restricted selection of explanatory images is reported. As expected, the most striking performance is that the vanishing-field region expands considerably now, in the sense that the rear of the body becomes fully unexposed (Figure 8b), while the frontal surface is overstressed somewhere (Figures 8a, c and d).

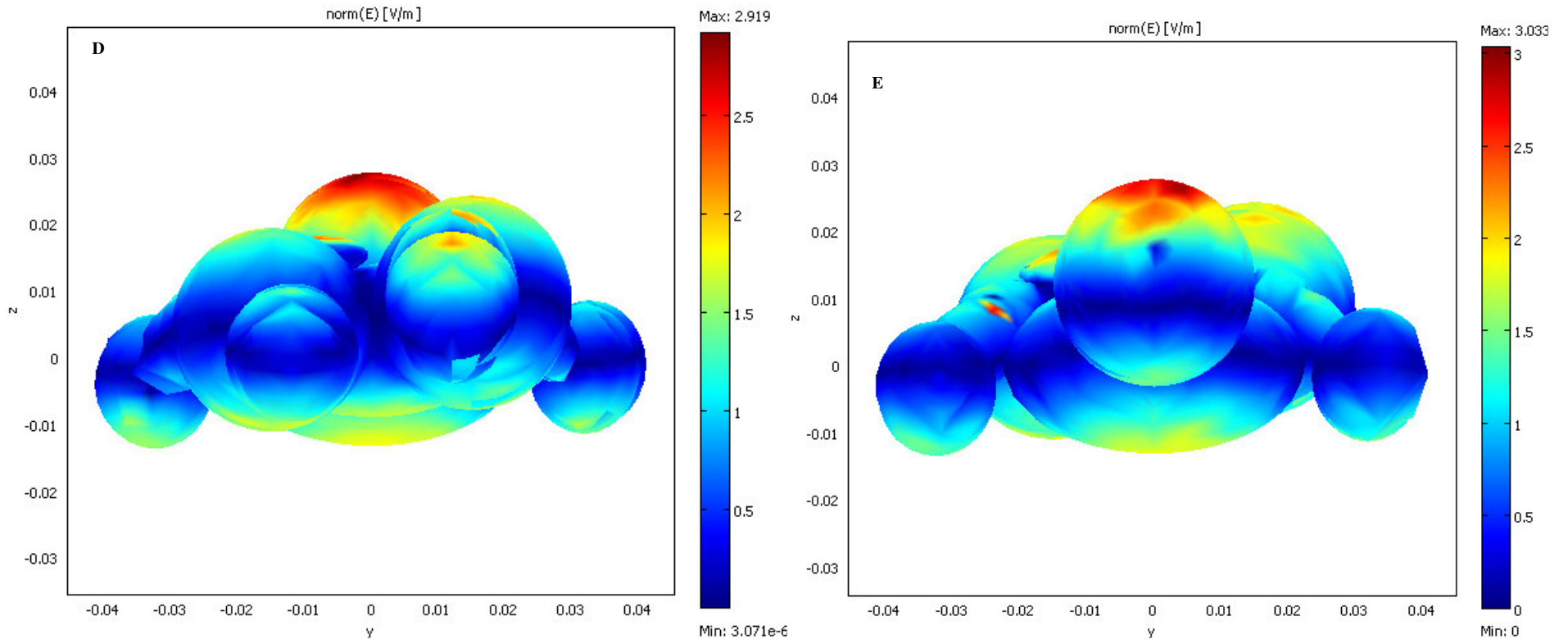


Figure 7. Contd.

Also as shown in Figure 9 the endogenous-field case is instructive specifically that in which the mannequin assumes the role of an isolated field source in the space where the background field is zeroed. Distinctive of the present circumstance is that the vanishing-field loop discussed for the suspended case of Figure 7 disappears. Instead, a significant surface field is present on either side of the body and, with larger magnitude, at the poles. In other words, the elemental regions variously contribute to the field formation all around the body, especially in function of their local prominence. As clearly depicted in Figure 9c,

the skull-cap experiences special overstress. Of course, this case is somehow similar to the single-ellipsoid one previously treated in “source”.

DISCUSSION

With reference to a diffusely reflecting/emitting general object, a careful analysis leads to prove how a local E-field can assume a structure but similar to that of a surface electrostatic field. In fact, although light is a form of electromagnetic radiation, the irradiating scenario is rather

governed by the same Laplace equation that usually applies to static or steady fields. To reconcile this apparent conflict between static and radiating fields, keep in mind that the material reaction to an excitation field generally involves power exchanges. In the case of light, such exchanges are governed by time averaged, substantially time-independent radiometric quantities subject to surface Laplacian-field distributions, even though the primary excitation field of course propagates according to radiation laws. As a result, a recorded field pattern is likely to be mistaken with that left by any strong luminous

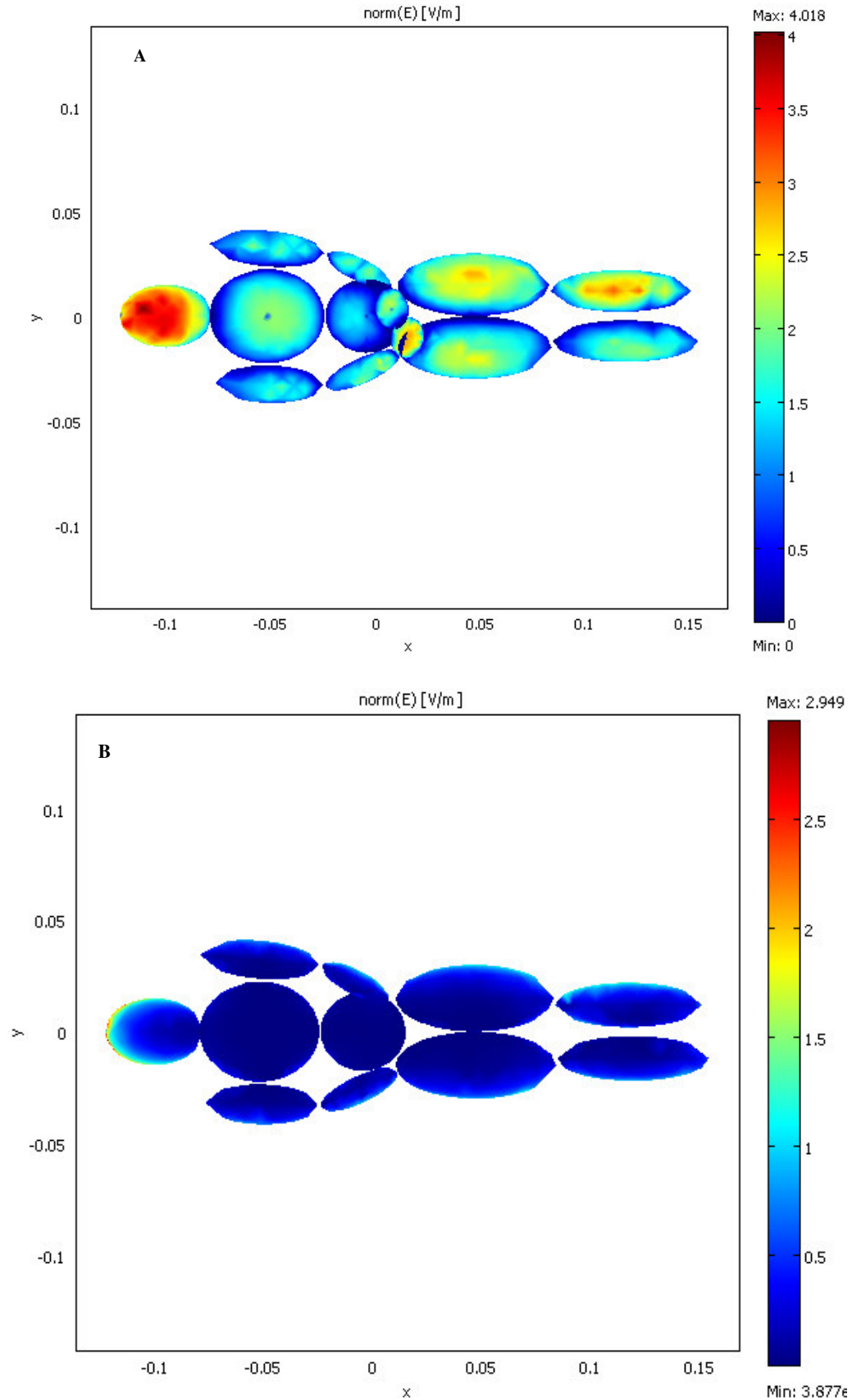
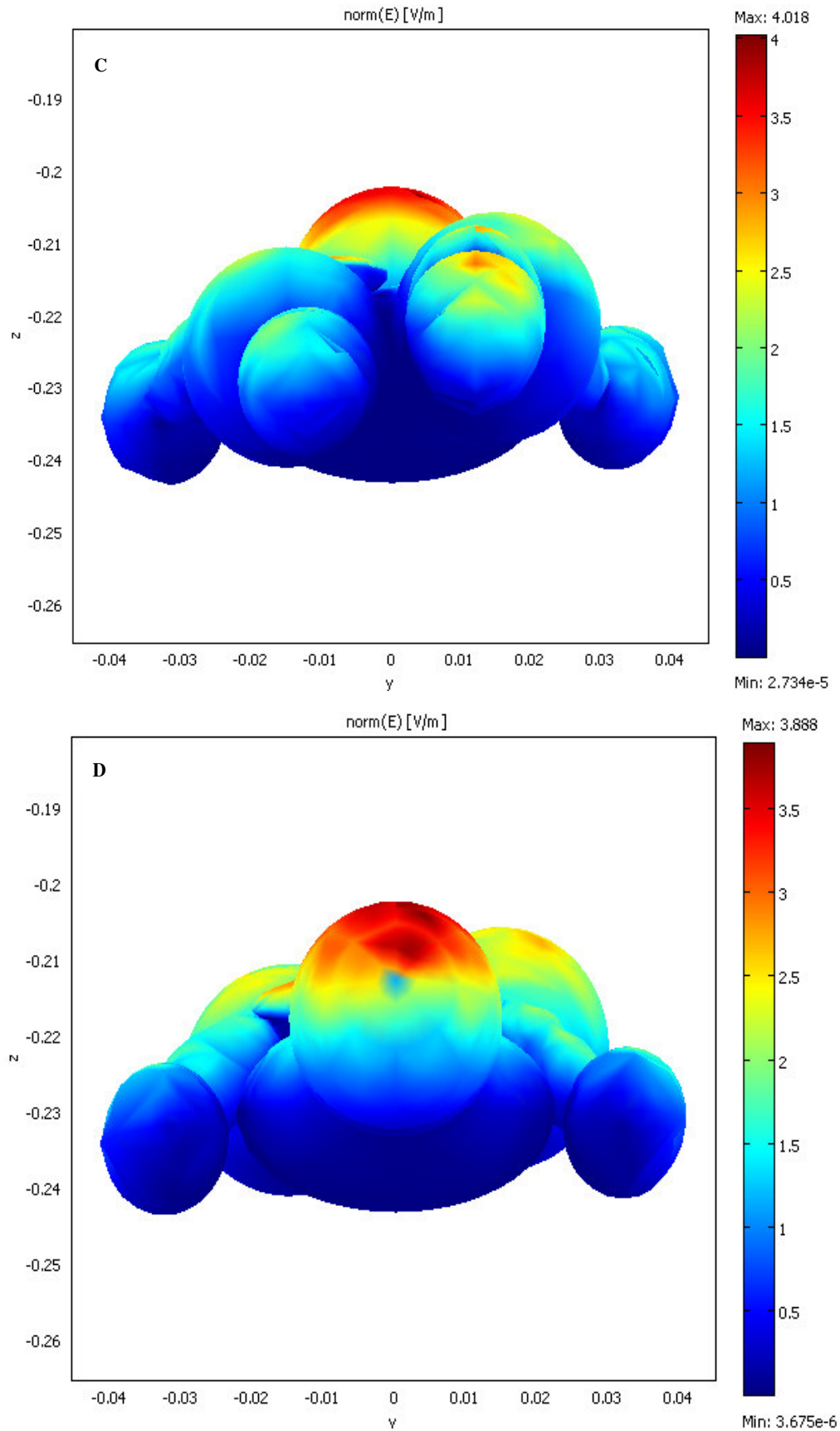


Figure 8. Case study: Grounded body lying on an indefinite plane and exposed as in Figure 7.



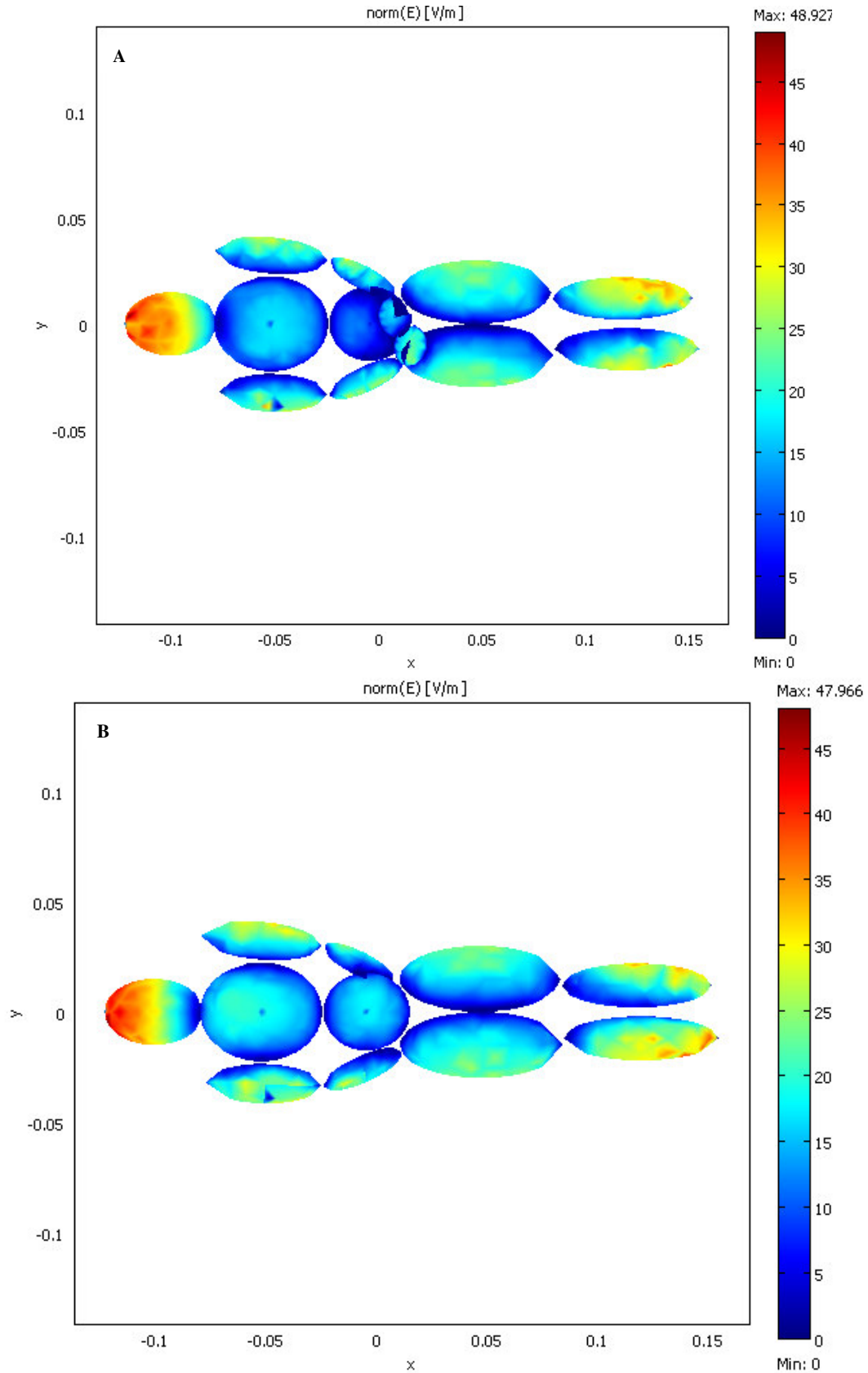


Figure 9. Case study: Isolated body as a charged conductor (field-source case). Vanishing background field; charging voltage 1 V.

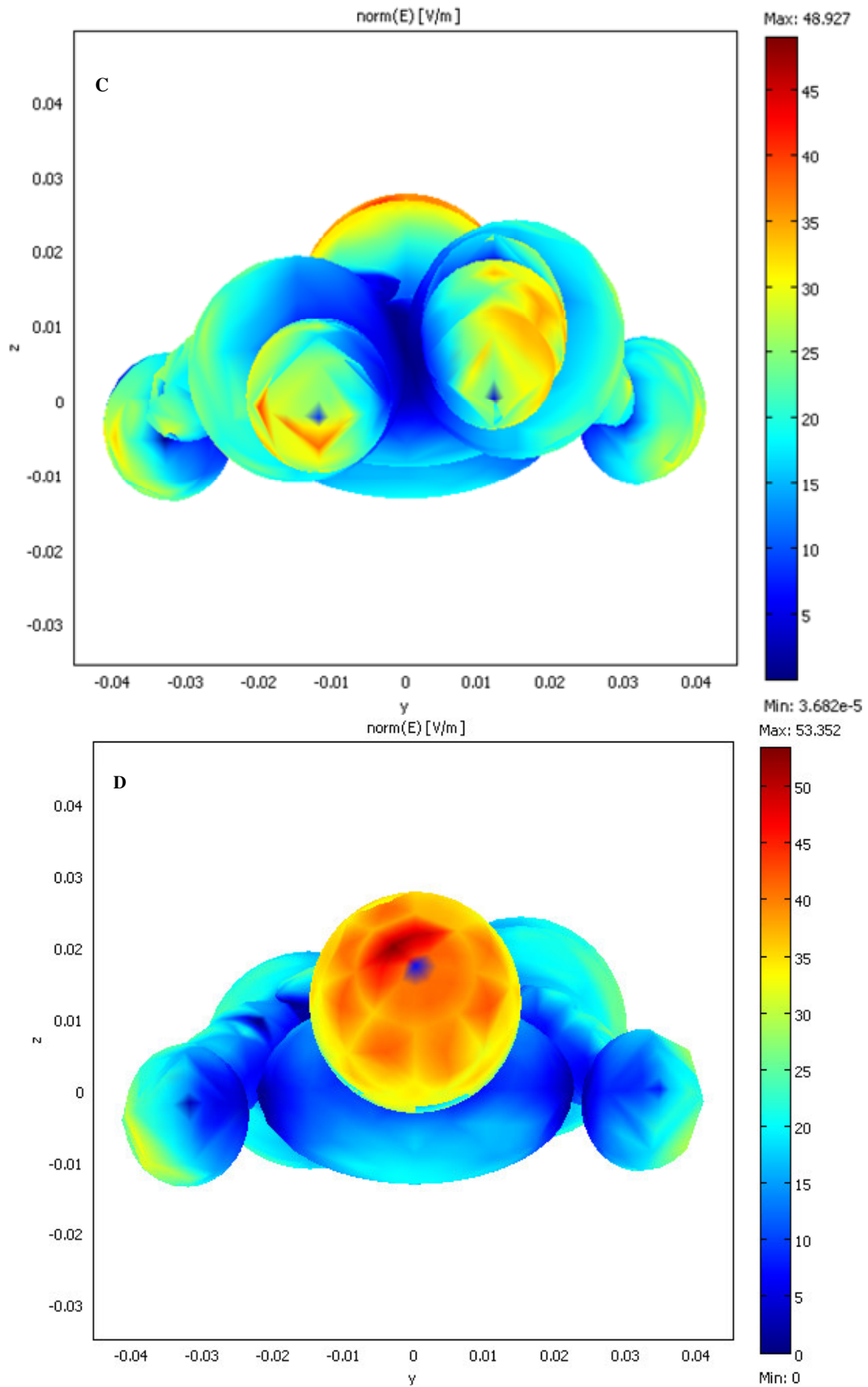


Figure 9. Contd.

radiation, even though the primary excitation field is an electrostatic one in the reality.

Reproducing a stable electrostatic impression of conducting surfaces by contact with sensitive films is a straightforward practice where the electrostatic discharge assumes the role of imaging agent (Kwark et al., 2004). The impression can be recorded on the inner side of an ordinary dielectric sheet that envelopes the object under ESD. The latter results in non-equilibrium, non-uniform zero-net charge plasma is especially confined on the overstressed protrusions of the conductor where the electric field tries to exceed a certain onset level. An effective corona activity is not easy to trigger, especially owing to the relatively high onset level determined by usual ambient conditions. However, under special circumstances hereinafter specified and pertaining to the present investigation, even a discharged conductor embedded in an electric field of moderate strength can be surrounded by a corona plasma. The image-forming mechanism becomes very effective when a significant preionization is present in the ambient gas, owing, for instance, to a suitable rate of radioactivity (de Liso, 2010; Loeb, 1965). Provided such conditions are met, vivid glow-type plasmas can be triggered even in the presence of relatively weak background fields. An additional remark is that the body is steadily surrounded, inside and beyond the plasma layer, by free charges of opposite polarities whose densities keep each other in approximate balance. Consequently, the macroscopic, smoothed-out electric field that ultimately controls the imprinting effect holds Laplacian, a crucial prerequisite for a truly electrostatic pattern to bear formidable resemblance to that of a hypothetical lightwave impact.

TS imaging

A seismic event can be preceded, accompanied or followed by some subsidiary phenomena giving rise to rather persistent electric fields, the magnitudes of which sometimes attain the order of some tens of kV/m. This is the case when underground piezoelectric effects occur, often associated with release of radon. Indeed, the present investigation pays, by elimination, special attention to the latter observable alone since:

- i) Due to upward effluxes of radioactive gas, the ambient air ionization significantly reduces the corona threshold and gives rise to background Laplacian electric fields even of two or three orders of magnitude less, as experimentally verified (de Liso, 2010);
- ii) Piezoelectric effects are inadmissible in the present description stated in the incompatible nature of Jerusalem subsoil;
- iii) East Jerusalem (The Old City) is categorized as a radon-prone area (the most critical type of radon invaded area) with an indoor concentration of 92.3 Bq/m^3 (almost

twice as high as the national average value) (Haquin et al., 2006; Shirav et al., 1997).

Distinctive of radon-prone areas subject to earthquake is appearance of pronounced indoor overconcentration with peaks of several orders of magnitudes greater than the usual level. This is due to abundant emissions of radon capable to trigger surface ESD even on conducting surfaces with slight curvature (exactly as in the case for the human model shown in Figure 7). This is because, different from normal ambient-radioactivity conditions, the growing radiation-originated ionization current gives local rise to significant space-charge distortion of the applied electric field. As a matter of fact, ESD threshold phenomena seemingly disappear under the described special circumstances (Loeb, 1965) and the ESD can naturally arise as an effect of local amplification of the background electric field, even when the latter hardly reaches the order of some hundreds of V/m (de Liso, 2010). Radon is a radioactive gas that can ionize a cavity in such a way that a significant amount of bipolar (zero-net space charge) ionization occupies most of the available ambient volume. However, charge accumulations, deposited with opposite polarities in proximity to the floor and vault of the cavity, behave as sources of a background electric field. The Laplacian character of such a macroscopic field is ensured by a zero-net-charge in the large inner space where the body is introduced. The charged clouds on the boundary can be explained in consideration of the different mobility of the involved ionic species, often subject to convective motions and/or upwardly directed thrusts caused by sulphureous throws. The described dipole model can approximately be assumed steadily provided efflux of radon is continuous and capable to counterbalance charge recombination/depletion mechanisms.

Overall, the above premises can be adopted to briefly explain how the TS imaging can result to a reasonable course of events. After having been introduced into a sepulchral cavity that was later closed, the wrapped body happened to experience the electrostatic effects of a vertically-oriented earthquake-originated electric field. In particular, the latter was caused by formation of ionized clouds in the closed ambient in consequence to radon efflux. Irrespective of being in intimate contact with or in close proximity to the corpse, the linen is found completely immersed in a plasma layer surrounding the enclosed corpse. The cover was exposed on the inner side to highly efficient corona chemical reactors, the distribution of which strictly depended on the local severity of the filamentary plasma. This varying discharge property was in turn controlled by the actual electric-field strength on the surface of the conducting corpse. Linen and laying support slightly influenced, in a comparative sense, the actual surface field, the latter being especially dictated by the exposure circumstances of the corpse itself. A surprising effect was the seemingly undistorted information transfer, later perceived by planar observa-

tion, from the 3D body onto the inner surface of the cover.

The above brief report approximately evokes the floating-body model treated in “ellipsoid” and displayed in Figure 7. In fact, the corpse was geometrically positioned above, thus electrically disconnected from, the positive cloud laying on the ground and significantly distanced from the negative counterpart on the vault. The computational error of neglecting the influence of the suspending system is estimated to be either comparable with the approximation error due to the human model adopted or within the uncertainties affecting this kind of investigation. In particular, any attempts aimed at carefully reproducing the actual burial conditions result in an arbitrary exercise owing to the considerable number of unknowns implied. However, the impressive mechanism was capable, as carefully illustrated hereinbefore in “theoretical examples”, to somehow render the human body, even if the cover presumably fitted the corpse all around by virtue of an outermost bandage (Lattarulo, 1998). Apart from some second-order features, the TS's frontal and dorsal figures appeared substantially undistorted, even due to their restricted transversal extension. This important feature is clearly shown in Figure 7 where the bluish vanishing-field loop is to be interpreted as a non-image zone.

SUBSIDIARY EVIDENCES

Even though based on visual perceptions invariably running the risk of subjectivity (Murra et al., 2010) or of being somewhat speculative, several issues are giving complementary support to the above electrostatic interpretation. Among these, it seems of considerable importance the discussion on the TS man's face impressed on both the inner and outer sides of the linen (Fanti et al., 2004). The pair of corresponding figures can very likely be explained according to the above electrostatic description. In fact, a typical corona performance consists in the possible restart of a number of filamentary streamers, aligned with the just originated ones, beyond thin dielectric barriers. As a result, the material bulk is left substantially unaffected since the energies otherwise required for a complete perforation of the material largely exceed those pertaining to corona activity. In other words, a barrier immersed in corona plasma usually results internally unaffected and externally exposed to chemical threat on both the delimiting sides, even though a lesser degree of aging is expected to manifest on the outer side. Further arguments in favor of a corona-originated transfer mechanism could be represented by second-order marks presumably regarding some objects placed in intimate contact with the corpse; this could be the case for coins and floral images perceived by some investigators (Filas, 1983; Balossino, 1997; Danin, 2010) – or externally attached to the linen. The latter case refers to a lately interpreted official report

on the corpse identification and treatment (Frale, 2009). According to the author, it is likely that the certificate was traced by *chalcànthos*, a marking ink that contained metallic components. Owing to such a conductive solute, the electrostatic influence exerted by the script on the plasma morphology could explain the inner reproduction of some words all around the face of the human figure.

Lastly, special attention has so far been paid to the images of the hair, beard and moustache because of their soft appearance.

Since admission made here on corpse was supine and the electrostatic agent was too weak to directly cause electrostatic piloerection, then the ion wind produced in the plasma gives, by elimination, a reasonable explanation for the above observations, consider the fact that an extensive investigation on the corona ion wind (somewhere referred to as electric wind) (Goldman et al., 1985) is especially being performed in avionics for producing considerable air jets by low-power sources of moderate electric fields (Font, 2006; Magnier et al., 2007).

CONCLUSIONS

The very intent of this paper is that of giving sound arguments in hopes of definitively settling the matter, thus warning against questionable interpretations of the image-forming process. This is because there are still a large number of those who insist in connecting the features of the TS image to light (or any further form of radiation) without supplying persuading motivations. Instead, adopting the working hypothesis of a natural electrostatic origin for the human image impressed on the TS appears to be an admissible enterprise. This hypothesis is sustainable especially in consideration of the radon-prone characterization of The Old City of Jerusalem, the experimental figures obtained elsewhere in similar radon-invaded areas as precursory evidences of seismic events and the encouraging theoretical results given and discussed in this paper. In spite of the lack of full experimental substantiation, the inherently non-radiating (from a rigorous electromagnetic standpoint) nature of the described mechanism presently meets all the basic physicochemical requirements and, therefore, looks reliable with special regard in the future.

REFERENCES

- Adler AD (2002). Chemical and physical aspects of the Sindonic images. The Orphaned Manuscript, D. Crispino Publisher (Effatà), Italy.
- Balossino N (1997). L'immagine della Sindone, ricerca informatica e fotografica, Elle Di Ci- Leumann Publisher, Italy.
- Beckmann P, Spizzichino A (1987). The Scattering of Electromagnetic Waves from Rough Surfaces. Artech House, Norwood (MA), p 396.
- Danin A (2010). The story of floral images on the Shroud of Turin. Danin Publishing, Jerusalem.
- De Liso G (2010). Shroud-like experimental image formation during natural electrostatic discharges. In Di Lazzaro P (ed). Scientific

- Approach to the Acheiropoietos Images: Proceedings of an International Workshop held at Frascati, Italy, pp. 11-18.
- Fanti G (2010). Can corona discharge explain the body image of the Turin Shroud? *J. Image Sci. Tech.* 54 (2): 020508-1-11.
- Fanti G, Basso R, Bianchini G (2010). Turin Shroud: compatibility between a digitized body image and a computerized anthropomorphic manikin. *J. Image Sci. Tech.* 54(5): 050503-1-8.
- Fanti G, Botella JA, Crosilla F, Lattarulo F, Svensson N, Schneider R, Whanger A (2010a). List of evidences of the Turin Shroud. In Di Lazzaro P (ed). *Scientific Approach to the Acheiropoietos Images: Proceedings of an International Workshop held at Frascati, Italy*, pp. 67-75.
- Fanti G, J.A. Botella JA, Di Lazzaro P, Heinburger T, Schneider R, Svensson N (2010b). Microscopic and macroscopic characteristics of the Shroud of Turin image superficiality. *J. Image Sci. Tech.* 54 (4): 040201-1-8.
- Fanti G, Maggiolo R (2004). The double superficiality of the frontal image of the Turin Shroud. *J. Opt. A: Pure Appl. Opt.* 6: 491-503.
- Font GI (2006). Boundary layer control with atmospheric plasma discharges, *AIAA J.* 44(7): 1572-1578.
- Filas FL(1983). The identification of Pilate coins on the Shroud. *Sindon. Dec.* 65-73.
- Frale B (2009). *La Sindone di Gesù Nazareno*. Il Mulino, Italy, p. 100.
- Goldman M, Goldman A, Gatellet J (1995). Physical and Chemical Aspects of Partial Discharges and Their Effects on Materials, *IEE Proc.-Sci. Meas. Technol.* 142(1): 11-16.
- Goldman M, Goldman A, Sigmond RS (1985). The corona discharge, its properties and specific uses. *Pure Appl. Chem.* 57(9): 1353-1362.
- Haquin G, Riemer T, Shyamai Y, Margalot M, Shirav-Schwartz M, Kenett R (2006). Radon Survey of Israel. *Nuclear Societies in Israel: Proceedings of a Conference held on Dead Sea*.
- Kwark C, Lee CW (1994). Experimental Study of a Real-Time Corona Discharge Imaging System as a Future Biomedical Image Device. *Med. Biol. Eng. Comp.* 32(3): 283-288.
- Langton NH, Davy N (1953). The two-dimensional magnetic or electric field above and below an infinite corrugated sheet. *Br. J. Appl. Phys.* 3: 134-158.
- Lattarulo F (1998). L'immagine sindonica spiegata attraverso un processo sismo elettrico. *Proc. III Congresso Internazionale di Studi sulla Sindone (Centro Internazionale di Sindonologia, Torino)* held at Torino, Italy.
- Lattarulo F, Amoruso V (2011). Electromagnetic treatment for the inverse reflectance-based shape recovery problem. *Int. J. Appl. Electromagnetics Mech.* 37 (2,3): 231-240.
- Loeb LB (1965). *Electrical Coronas*, Univ. of California Press, Berkeley, p. 74.
- Magnier P, Hong D, Leroy-Chesneau A, Bauchire JM, Hureau J (2007). Control of separated flows with the ionic wind generated by a DC corona discharge. *Exp. Fluid.* 42: 815-825.
- McAllister IW (1990). Conductor Curvature and Surface Charge Density. *J. Phys. D: Appl. Phys.* 23: 359-362.
- Mosteller RD (1987). Simplified calculation of body surface area. *N. Engl. J. Med.* 317(17): 1098.
- Roth A (1959). *Hochspannungstechnik*. Springer-Verlag, Wien, Austria. Cap. I, Sect. 23.
- Murra D, Di Lazzaro P (2010). Sight and brain: an introduction to the visually misleading images. In Di Lazzaro P (ed). *Scientific Approach to the Acheiropoietos Images: Proceedings of an International Workshop held at Frascati, Italy*, pp. 31-34.
- Shirav M, Vulkan U (1997). Mapping radon-prone areas – a geophysical approach. *Environ. Geol.* 31: 3-4.
- Stratton JA (1941). *Electromagnetic Theory*. Mc Graw-Hill, New York, p 131.
- Van Brunt RJ (1994). Physics and Chemistry of Partial Discharge and Corona – Recent Advances and Future Challenges. *IEEE Trans. on Dielectrics and Electrical Insulation* 1(5): 761-784.
- Waters RT (1982). Spark breakdown in non-uniform fields. In Meeks JM, Craggs JD (eds). *Electrical breakdown of gases*, John Wiley, New York.